Journal of Geodesy (1998) 72: 161–178

Journal of Geodesy

Improvement of the empirical thermospheric model DTM: DTM94 – a comparative review of various temporal variations and prospects in space geodesy applications

C. Berger[1], R. Biancale[2], M. Ill[3], F. Barlier[1]

[1] Observatoire de la Côte d'Azur, Groupe de Recherche de Géodésie Spatiale, Avenue Copernic, F-06130 Grasse, France
Tel.: + 33 493 405353; e-mail: berger@obs-azur.fr
[2] Observatoire Midi Pyrénées, Groupe de Recherche de Géodésie Spatiale, 14 Avenue Edouard Belin, F-31400 Toulouse, France
[3] Budapest Observatory, Hungary

Received: 3 December 1996 / Accepted: 4 August 1997

Abstract. The Drag Temperature Model (1978) has been improved to respond better to the actual requirements of space geodesy, especially under extreme solar and geomagnetic conditions. Extended data and an improved algorithm have been considered, leading to valuable improvements. Temporal variations of temperature of the thermopause, total density and major chemical constituent density are reviewed and compared to the DTM94, DTM78 and MSIS86 models. A comparison with data is performed, giving the mean ratios between observed and model values with their root mean squares for different physical and geometric conditions. This comparison is made for the three models and includes data used in the modelling as well as external data. The limits of the thermosphere modelling are discussed.

Key words. Thermosphere models · Non-gravitational forces · Air drag · Orbit determination · Space geodesy

1 Introduction

During recent years, significant progress has been made in modelling forces acting on an artificial satellite as well as in tracking systems by laser or by radio techniques; e.g. GPS (Global Positioning System), DORIS (Doppler Orbit determination and Radio positioning Integrated by Satellite), PRARE (Precise Range And Range-rate Equipment). Such progress has entailed very significant improvement in trajectography determination and in many fields related to space geodesy. For example, in the case of TOPEX/POSEIDON (oceanographic satellite) at an altitude of 1336 km, the error in the radial direction is only of about 2–4 cm (Nouël et al. 1994, Tapley et al. 1994, Smith et al. 1996) and the error induced by mismodelling of the atmospheric drag is less than 1 cm, by estimating empirical air drag coefficients (Marshall et al. 1995). At the altitude of ERS-1 and ERS-2 (Earth Remote Sensing satellites), about 800 km, the situation is a little different because of the lower altitude and greater perturbating effects. Nevertheless, thanks to the possibility of fitting empirical drag-scale factors (f_d) and to cross-over difference techniques applied to altimeter data, the error in the radial direction is only about 10 cm or less (Scharroo et al. 1993). In the case of geodetic satellites covered with laser retro-reflectors, such as STARLETTE, the improvement of the precision of the trajectory determination is also quite significant, at sub-decimetric levels (Schwintzer et al. 1997). The quality of the orbit determination is very much dependent on the number of drag-scale factors to be determined (Ries et al. 1993). Nevertheless, it does not mean that any effort in atmospheric modelling is without interest. So, the present paper focuses on the modelling of atmospheric drag forces and on empirical thermospheric models for different purposes.

The role of a possible improvement in air-drag modelling has to be attempted in the context just described. For practical reasons we have chosen a classical approach, although from this point of view the previous efforts to improve the empirical models from concepts already used in Jacchia (1971) or in Hedin et al. (1974) have recently been estimated to be a little disappointing. Indeed, a kind of limit could have been reached in the actual concept of empirical modelling (Marcos et al. 1994). But the comparison of observed density data with predicted values by models generally exhibits discrepancies and biases, as already indicated by Gaposchkin and Coster (1986) and Hedin (1988). With new data and more elaborate algorithms, progress could be expected according to different criteria to be defined as a function of objectives searched for: orbit determination, gravity field determination, oceanography, geophysical interpretation and prediction of satellite motion.

Correspondence to: C. Berger

These remarks had us to improve the DTM model (Drag Temperature Model) developed in 1978 (Barlier et al. 1978); in particular, to represent more correctly extreme solar and geomagnetic conditions. We know the parameters were not satisfactorily modelled for these conditions because, at this epoch, the amount of available thermospheric data was insufficient. This fact has entailed some biases in the represention of atmospheric effects. However, the satisfactory modelling of the total density for moderate solar conditions made this model useful for various applications: trajectory computation for satellites such as SPOT or TOPEX/POSEIDON at the S.O.D. (Service d'Orbitographie Doris) in CNES (Nouël et al. 1994) or at Delft (Smith et al. 1996), development of gravity models such as JGM1 and 2 (Nerem et al. 1994) or GRIM4-S4 and GRIM4-C4 (Schwintzer et al. 1997). It is also of interest to have the DTM model with its own specification with a precision at the level of the international reference model MSIS (Hedin 1987) for any solar conditions. In merging new data, comparison between models can reveal the order of magnitude of biases to be expected in thermospheric modelling.

In Sect. 2, the new solution for DTM is presented, labelled DTM94 (94 is the computation year). In Sect. 3 a comparative review of most important effects of total density variations is presented for the MSIS86, DTM (labelled later as DTM78) and DTM94 models. Then observations are compared with predicted values by these models, including observations not used in DTM94 model development, and finally remarks are given on the limitations in modelling and on prospects in the field related to space geodesy and its applications.

2 Model DTM94

2.1 DTM94 algorithm

The DTM78 model (Barlier et al. 1978) was developed at the Centre d'Etudes et de Recherches Géodynamiques et Astronomiques (CERGA, France) in a cooperative effort with the Institut d'Aéronomie Spatiale in Belgium (G. Kockarts) and the Service d'Aéronomie du CNRS in France (G. Thuillier). The model was based on the hypothesis of independent static diffuse equilibrium of different thermospheric constituents: H, He, O, N_2, O_2 as adopted in other previous thermospheric models (Jacchia 1971; Hedin et al. 1974). The differential equation of diffuse equilibrium leads, by integration, to the concentration of each major constituent according to the altitude law:

$$f_i(z) = (T_{120}/T(z))^{1+\alpha+\gamma_i}\exp(-\sigma\gamma_i\zeta)$$

where the different parameters are defined as follows:

T_{120}: temperature at 120 km (lower limit of the model),
$T(z)$: temperature at the altitude z above the standard ellipsoid according to the Bates temperature profile (Bates 1959): $T(z) = T_\infty - (T_\infty - T_{120})\exp(-\sigma\zeta)$
T_∞: temperature of the thermopause,
α: thermal diffusion coefficient for H and He (-0.38 if not 0) (Kockarts 1963)
γ_i: $m_i g_{120}/(\sigma k T_\infty)$
k: Boltzmann constant ($k = 1.3803\,10^{-23}\,\mathrm{JK}^{-1}$),
g_{120}: acceleration of gravity at 120 km,
m_i: molecular mass,
σ: relative vertical temperature gradient $T'_{120}/(T_\infty - T_{120})$,
T'_{120}: vertical temperature gradient at 120 km,
ζ: geopotential altitude,
R: polar Earth radius (6356.770 km)

Both the thermopause temperature and the gas concentration evolve depending on season, solar local time, latitude and also as a function of the atmospheric heating process due to the solar electromagnetic radiations (characterized by the 10.7-cm flux) and due to the particle flow (represented by the geomagnetic activity index K_p). This dependence is modelled by an empirical function $G(L)$ (Hedin et al. 1974) for the thermopause temperature:

$$T_\infty = T_\infty^\circ(1 + G(L))$$

and for the concentrations:

$$n_i(z) = a_i^\circ \exp(G_i(L)) f_i(z)$$

and hence for the densities:

$$\rho_i(z) = m_i n_i(z)$$

T_∞° is a constant; it represents the averaged thermopause temperature for mean solar conditions and is denoted a_1 in Table 3; a_i° are constants for the major constituents (subscript i); they represent the mean concentrations of these constituents at 120 km and are likewise denoted a_1 in Table 3.

The expansion function $G(L)$ for model quantities is as follows:
Non periodic terms:
Latitude:

$$a_2 P_{20} + a_3 P_{40} + a_{37} P_{10}$$

Solar activity:

$$+ a_4(F - \bar{F}) + a_5(F - \bar{F})^2 + a_6(\bar{F} - 150)$$
$$+ a_{38}(\bar{F} - 150)^2$$

Magnetic activity:

$$+(a_7 + a_8 P_{20})K_p +$$

either $a_{39}\exp(K_p)$ for the temperature or $a_{39}K_p^2$ for the neutral constituents.
Periodic terms:
Symmetrical annual:

$$+(a_9 + a_{10}P_{20})\cos[\Omega(d - a_{11})]$$

Symmetrical semi-annual:

$$+(a_{12} + a_{13}P_{20})\cos[2\Omega(d - a_{14})]$$

Asymmetrical annual (seasonal):

$+(a_{15}P_{10} + a_{16}P_{30} + a_{17}P_{50})\cos[\Omega(d - a_{18})]$

Asymmetrical semi-annual:

$+a_{19}P_{10}\cos[2\Omega(d - a_{20})]$

Diurnal

$$+\big(a_{21}P_{11} + a_{22}P_{31} + a_{23}P_{51} + (a_{24}P_{11} + a_{25}P_{21})\cos[\Omega(d - a_{18})]\big)\cos\omega t$$
$$+\big(a_{26}P_{11} + a_{27}P_{31} + a_{28}P_{51} + (a_{29}P_{11} + a_{30}P_{21})\cos[\Omega(d - a_{18})]\big)\sin\omega t$$

Semidiurnal:

$$+(a_{31}P_{22} + a_{32}P_{32}\cos[\Omega(d - a_{18})])\cos 2\omega t$$
$$+(a_{33}P_{22} + a_{34}P_{32}\cos[\Omega(d - a_{18})])\sin 2\omega t$$

Terdiurnal:

$+a_{35}P_{33}\cos 3\omega t + a_{36}P_{33}\sin 3\omega t$

P_{nm} are the non-normalized Legendre associated functions (see Barlier et al. 1978). F is the solar radio flux at 10.7 cm on the previous day, $\bar{F}$ is the average F over three solar rotations (81 days) before the required day, K_p is the three-hourly geomagnetic index taken with a delay depending on latitude (3 h at the pole, 6 h at the equator with a linear interpolation), d is the day of the year, $\Omega = 2\pi/365$ (day^{-1}), $\omega = 2\pi/24$ (h^{-1}). In the case of leap years, the value Ω is not totally correct, but its effect is much smaller than the error in the model, and has been ignored. All the periodic terms are to be multiplied by (1 + terms of solar activity) except for H and He.

2.2 DTM94 data

The original idea in the DTM78 model was to determine the main atmospheric constituents (N_2, O, He) using the temperature model of Thuillier et al. (1977) and total density data in a large range of altitudes between 160 and 1500 km. Indeed, each main constituent is successively prevalent in concentration, so that an iterative process can be used to determine, over a certain interval of altitude, molecular nitrogen, atomic oxygen and then helium. Iteration yields a good representation of total density by addition of the main constituents. Details can be found in Barlier et al. (1978). On the other hand, molecular oxygen and hydrogen have to be taken elsewhere from the MSIS model (Hedin et al. 1977). Their effect is generally more limited as far as the air drag is concerned, except for the hydrogen at the low solar activity level. It is another approach with respect to studies in which total density is directly modelled (e.g, Volkov 1984; Sehnal 1990).

For the purpose of improving the model, new data (total densities, temperatures and also chemical components) have been added, in particular, for extreme solar conditions. Information on data used in the modelling is given in Table 1. The histograms of the repartition of data as a function of solar and geomagnetic activity are given in Fig. 1.

2.3 Merging data – data calibration

Data are affected by random errors and biases. For satellite drag data, when total density has to be estimated, difficulties arise. A first difficulty is linked to horizontal winds generally not known accurately [orders of magnitude of winds can be found in Hedin et al. (1991)]. The winds have not been taken into account for drag data processing. Another is due to the aerodynamic coefficient quantifying the momentum exchange between atoms or molecules with the satellite surface (Cook 1965; Afonso et al. 1985). It is very difficult to model this coefficient accurately. Errors of a few percent up to 15% or 20% are possible (Gaposchkin 1994). In our case, the reference has been defined by the balloon satellite data determined by Jacchia and Slowey (e.g. 1975) and from there a calibrating factor has been adjusted for each satellite from which total densities have been deduced.

Table 1. Summary of data sets

Data set	number of data	period (month · year)	altitude range (km)	references
Ogo-6 temperature Fabry-Perot interferometer	46500	06.69 → 08.70	230 → 290	Blamont and Luton (1972)
DE-2 temperature Wind and temperature Spectrometer	52000	08.81 → 02.83	200 → 600	Spencer et al. (1981) Killeen et al. (1988)
Temperature deduced from CACTUS accelerometer data	2500	01.76 → 06.76	Thermopause	Berger et al. (1986, 1988)
Total density Satellite drag	65000	01.61 → 12.73	160 → 1200	Jacchia (1971) Barlier et al. (1978)
Total density CACTUS accelerometer	63000	06.75 → 02.79	270 → 600	Villain (1980)
DE-2 N_2 density Neutral mass spectrometer	41600	08.81 → 02.83	200 → 500	Carignan et al. (1981) Hedin (1987)
DE-2 O density	52000	08.81 → 02.83	280 → 575	idem
DE-2 He density	73500	08.81 → 02.83	300 → 1000	idem

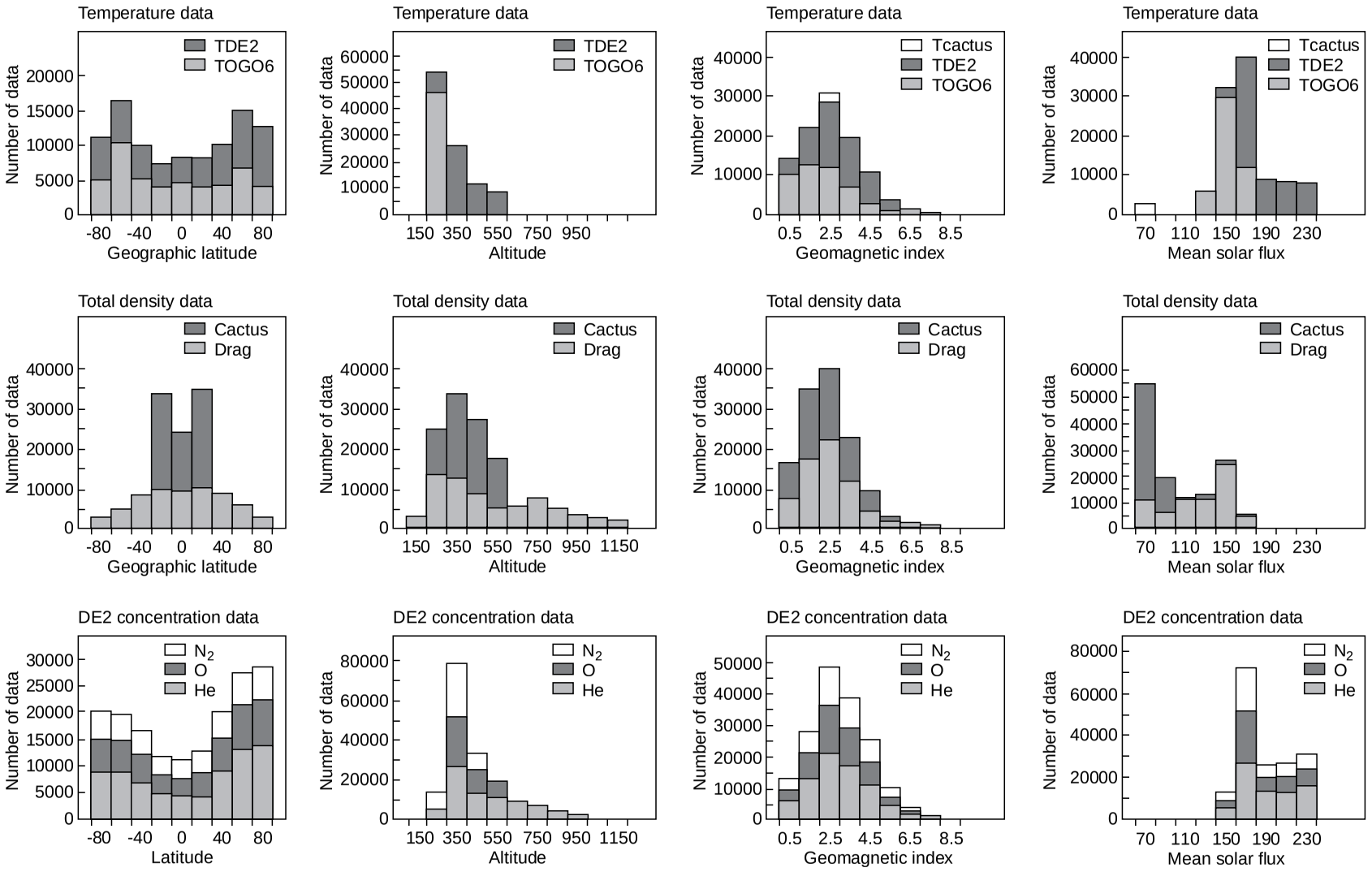

Fig. 1. Histograms of repartition of data as a function of solar and geomagnetic activity

Table 2. Calibration factors for spectrometric data

Neutral constituent	number of DE2 data used	altitude (km)	DE2 data to preliminary DTM model ratio	σ	Hedin (1987) calibration factor
DE-2 N_2	12650	250 → 500	0.70	0.26	0.60
DE-2 O	18380	280 → 575	0.91	0.24	0.89
DE-2 He	15500	350 → 750	0.86	0.28	0.86

Table 3. Coefficients a_i for the DTM94 model

Coefficient	T_∞	H	He	O	N_2
a_1	0.1000E 04	0.1761E 06	0.2791E 08	0.8472E 11	0.3204E 12
a_2	0.9461E−02	−0.1337E 00	0.1096E 00	−0.6645E−01	−0.1402E 00
a_3	0.4267E−01		−0.1908E 00	−0.9741E−01	0.5722E−01
a_4	0.1795E−02	−0.1246E−01	−0.2077E−03	0.1228E−02	0.1126E−02
a_5	−0.7990E−05		0.4835E−05	0.4498E−05	−0.2078E−05
a_6	0.3367E−02	−0.1930E−01	0.2112E−02	0.5358E−02	0.3424E−02
a_7	0.2263E−01	−0.6000E−01	0.2212E−03	0.2557E−02	−0.1159E−01
a_8	0.3786E−01	−0.2000E−01	−0.1617E 00	−0.9822E−01	0.5516E−01
a_9	−0.1923E−01	0.5878E−01	−0.9222E−01	0.1009E 00	−0.1005E−01
a_{10}	−0.9241E−02		−0.8301E−02	0.6261E−02	−0.4390E−01
a_{11}	−0.2107E 03	0.9227E 02	0.2135E 03	0.1156E 02	0.1959E 03
a_{12}	0.1032E−01		0.2350E 00	0.1760E 00	0.3248E−01
a_{13}	0.2886E−01		−0.7905E−01	−0.7128E−01	0.5650E−01
a_{14}	−0.7631E 02		0.1104E 03	0.1064E 03	0.8820E 02
a_{15}	−0.1850E 00	0.3301E 00	−0.1268E 01	0.3329E 00	0.2881E 00
a_{16}	−0.2031E−01	0.1045E 00	−0.1851E 01	−0.1145E 00	−0.3143E−01
a_{17}	0.1447E−01		0.6662E−01	−0.4242E−02	
a_{18}	−0.3631E 01	−0.1477E 02	−0.1870E 03	−0.6751E 00	−0.2001E 03
a_{19}	−0.2894E−01	−0.9065E−01	−0.4215E−01	−0.4171E−01	0.6070E−01
a_{20}	−0.1737E 03	−0.7200E 02	−0.2167E 03	0.1344E 03	0.5115E 02
a_{21}	−0.1082E 00	0.2094E−00	−0.1278E 00	−0.6593E−01	−0.4610E−01
a_{22}	−0.1999E−02	0.2830E−01	−0.6182E−02	−0.1934E−01	−0.9700E−02
a_{23}	0.3397E−02		−0.1745E−01	−0.8585E−02	0.3491E−02
a_{24}	−0.1613E−01	0.8571E−01	−0.4360E−01	0.8635E−01	
a_{25}	−0.9609E−02	−0.2475E−01	−0.5285E−01	0.8568E−01	
a_{26}	−0.1045E 00	0.3830E 00	0.3120E 00	0.4549E−01	−0.7333E−01
a_{27}	0.4575E−02	0.2941E−01	−0.2137E−01	−0.3872E−01	0.2116E−01
a_{28}	0.4584E−02		−0.2453E−01	−0.1287E−01	0.7033E−02
a_{29}	0.1776E−01	−0.3974E−02	−0.3673E−02	−0.9178E−01	
a_{30}	−0.4227E−02	0.4356E−01	−0.8833E−01	0.4262E−01	
a_{31}	−0.3567E−02		0.3399E−01	0.4339E−01	−0.6920E−02
a_{32}	−0.3606E−03		0.5131E−02	0.5689E−02	
a_{33}	0.1049E−01		−0.1474E−01	0.6651E−02	−0.7290E−02
a_{34}	0.4571E−02		0.8556E−02	−0.1017E−01	
a_{35}	−0.2175E−04		0.1957E−02	0.2706E−02	−0.2920E−02
a_{36}	0.1511E−02		−0.4503E−02	−0.4710E−02	0.2705E−02
a_{37}	0.2167E−02		−0.1024E 00	−0.1464E−01	−0.5994E−02
a_{38}	−0.1142E−05		−0.1687E−04	−0.6406E−05	
a_{39}	0.6582E−04		−0.1426E−02	0.1518E−02	0.8213E−02
Molecular oxygen O_2			0.4475E + 11 cm^{-3}		
Temperature at 120 km			380 K		
Temperature gradient at 120 km			14.348		

Dynamics Explorer 2 spectrometer data (kindly provided by A.E. Hedin) are also affected by some biases. Although calibration factors have been given by Hedin (1987), we have preferred to calibrate these data in an homogeneous way with total densities and then to compare them to Hedin's values. To accomplish this, a preliminary model DTM94 (using satellite drag and CACTUS data) has been developed for moderate solar and geomagnetic activity (F less than 170, K_p less than 4). Spectrometer data corresponding to the same solar conditions have been compared to concentrations predicted by this model. The results are given in Table 2 along with the number of data used for elaborating the preliminary model. The agreement is excellent except for molecular nitrogen, where a difference of 15% is exhibited. The solution with satellite drag data has been adopted for reasons of coherence. For generating the final model the calibration factors have been fixed at these values.

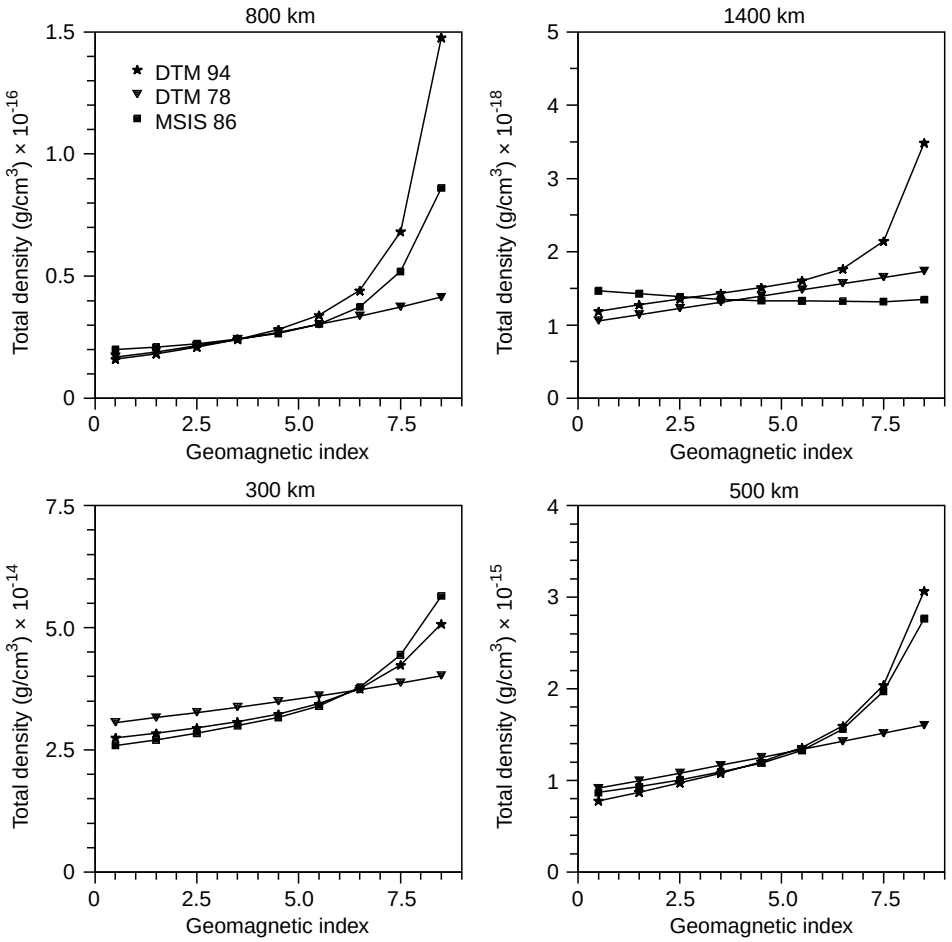

Fig. 2. Total density given by the three models studied for conventional conditions as a function of geomagnetic activity and altitude

It is also important when merging data sets to weight them properly and to select a reasonable number of data so that one type of data does not overwhelm the others. The number of data used for generating the new model is given in Table 1. The coefficients "a_i" of the final model (see Sect. 2.1), determined by a least-squares procedure applied over all the data set, are given in Table 3.

3 Temporal variations of thermospheric parameters – comparison between MSIS86, DTM78 and DTM94 models

The physical parameters of the thermosphere, temperature, concentrations and total densities undergo temporal variations. These types of variation are now well identified and can be predicted thanks to empirical models.

In view of geodetic applications, several altitudes have been selected to display the amplitude and the phase of main structures, namely 300, 500, 800 and 1400 km corresponding to such geodetic satellites as GFZ-1, CHAMP, ERS-1,2, TOPEX/POSEIDON. To estimate the existing differences between two given models several types of variation are successively considered and, in priority, effects linked to solar and geomagnetic activity in reason of significant discrepancies already mentioned. Mean conditions for parameters have been chosen conventionally (generally and according to the study to be performed, latitude: 45°N, longitude: 0°, local solar time: 9 h, day of the year: 80, mean solar flux and solar flux: 150 $10^{-22}\,\mathrm{Wm^{-2}\,Hz^{-1}}$, K_p: 3)

3.1 Variations linked to geomagnetic activity

A variation of the planetary index K_p from 0.5 to 7.5 yields an increase in total density which reaches its maximum value at 800 km (Fig. 2). Helium (Fig. 3) has a specific behaviour, since a decrease can be observed in the polar region, while an increase is observed at the equator (Barlier et al. 1979; Prölß 1980). This is due to the dynamics of the thermosphere, the light components such as helium being blown towards the equator during a strong geomagnetic event (Mayr and Volland 1973). As a result, at mid-latitudes the variation is small, changing from a decrease to an increase, and this fact can explain that at 1400 km where He prevails, MSIS86 and DTM94 appear to have an opposite behaviour in total density (Fig. 2). For the other parameters (T_∞, O, N_2), an increase is observed at mid-latitudes (Figs. 3 and 4a) generally in reasonable agreement except for very high K_p values (greater than 7.5), where differences can be observed, especially for DTM78. Here it is necessary

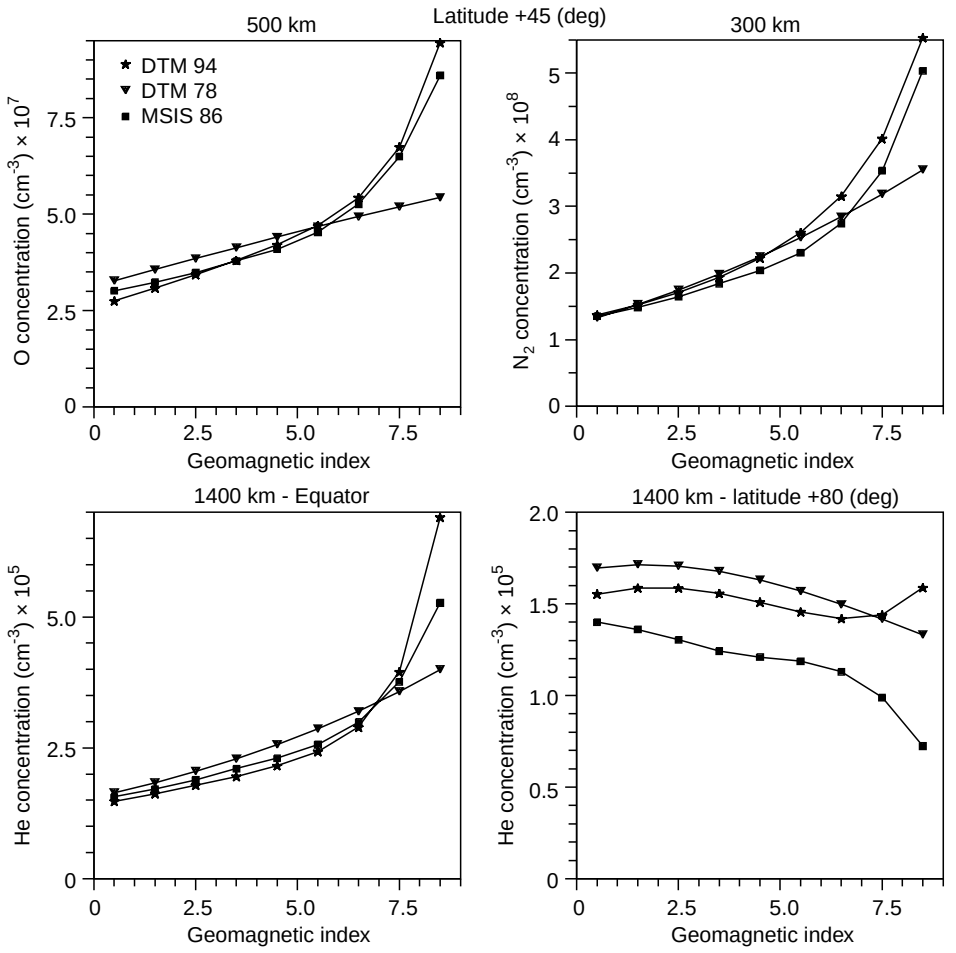

Fig. 3. Neutral composition given by the three models for conventional conditions as a function of geomagnetic activity and latitude

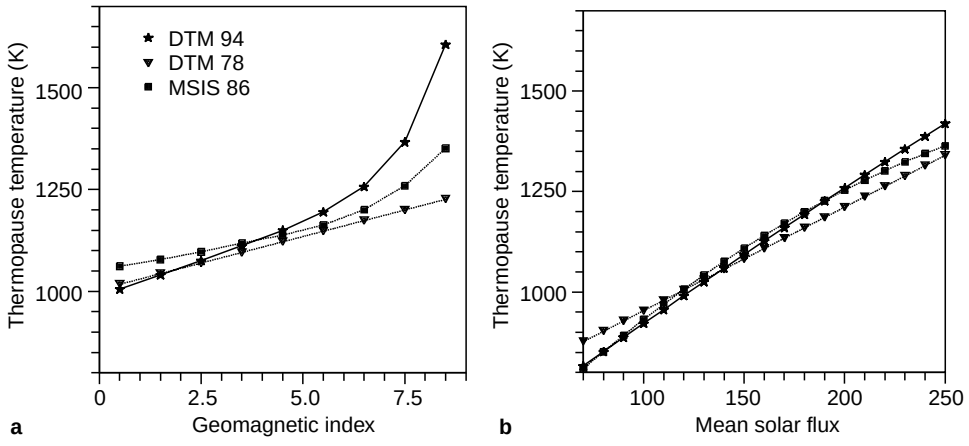

Fig. 4a, b. Thermopause temperature given by the three models as a function **a** of geomagnetic activity and **b** of mean solar flux

to mention that after the publication of DTM78 it was established that its predicted increase was too small, particularly at the equator. An empirical correction was applied to the atomic oxygen. Moreover, a hydrogen model, which is of importance above 1000 km for a low solar activity level, was added to the global model [taken from Hedin et al. (1977)]. The DTM78 model with these changes was labelled DTMH and remained unpublished, though it was widely used with success in orbit determination, such as for the SPOT and TOPEX/POSEIDON satellites (Nouël et al. 1994).

It is of interest to recall that variations with geomagnetic activity are dependent on other parameters such as mean solar flux and latitude. For example, the increase in temperature per unit of ΔK_p ranges from 20 K at the equator to 75 K in the auroral regions for the conventional conditions adopted in this section and the increase in total density at 500 km is twice as strong

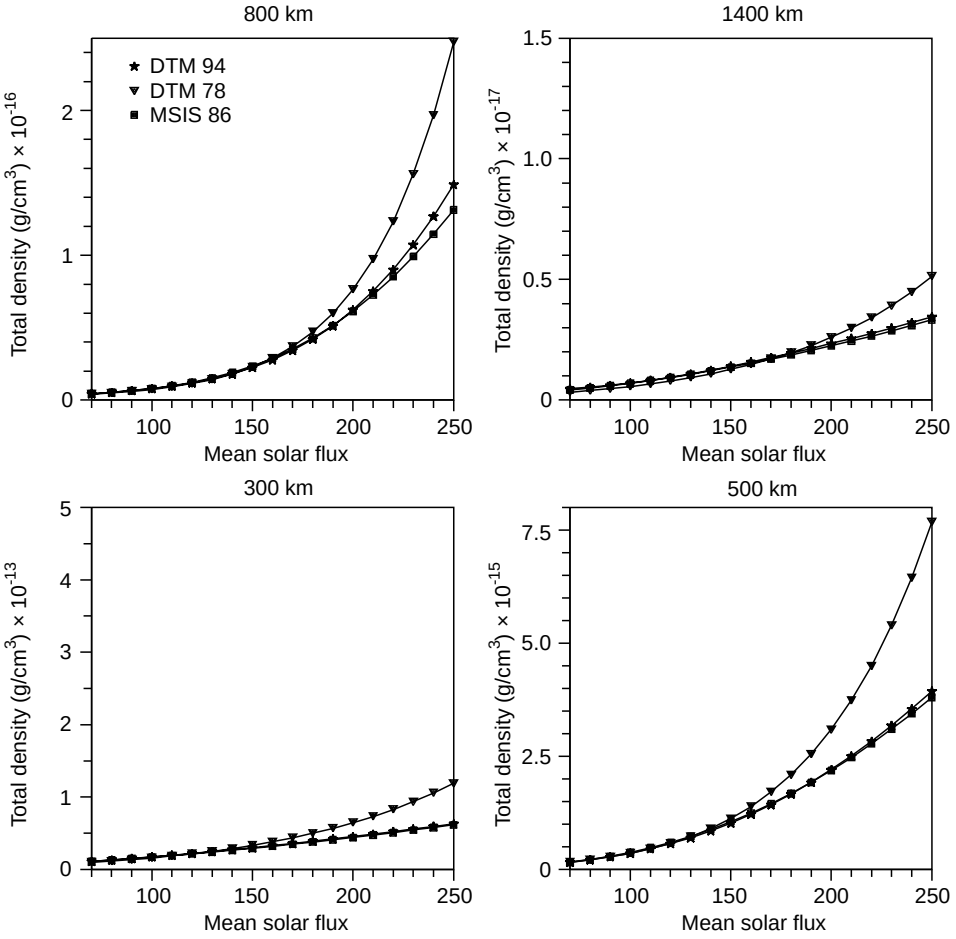

Fig. 5. Total density given by the three models studied for conventional conditions as a function of mean solar flux

for low solar activity level than for high solar activity level.

3.2 Variations linked to solar activity

The total density variations as a function of the mean solar flux $\bar{F}$ are displayed in Fig. 5. When $\bar{F}_{10.7}$ varies from 70 to 250, the *total density maximum to total density minimum* ratio reaches the values of 6, 25, 30 and 7 corresponding to the altitudes of 300, 500, 800 and 1400 km, respectively. The agreement is generally good between the models, except for DTM78, when the mean solar flux is greater than 180. This is due to the lack of very high solar activity data in generating this model, and indeed this constituted an important reason to add new data to the new version in order to improve it. The temperature increases by about 600 K for $\bar{F}$ varying from 70 to 250 (Fig. 4b).The agreement is very good for DTM94 and MSIS86 up to $\bar{F} = 200$. A specific mention has to be made for hydrogen. As shown by Kockarts and Nicolet (1963), its behaviour is opposite to that of the other components and exhibits its highest values for low solar activity levels. For example (Banks and Kockarts 1973), for a mean thermopause temperature of 750 K (low solar activity level) and for altitudes of 1000 and 2000 km, the concentration ratio H/He reaches values of 5 and 110, respectively. But for a mean temperature of 1250 K (high solar activity) these values are only 0.05 and 0.35. Therefore, the role of hydrogen is only of importance for a low solar activity level. This gives the reason why at 1400 km the variations of the total density are relatively diminished because of the opposite behaviour of He and H.

The mean solar flux represents the slowly varying component of the solar activity, but the quantity "$F_{10.7} - \bar{F}_{10.7}$" represents the instantaneous variation of this activity, which plays an important role in the temperature and density fluctuations, as is well known. The variations in temperature and in total density are given in Fig. 6 for two levels of solar activity corresponding to $\bar{F}_{10.7} = 100$ and 200. Some discrepancies can be observed for DTM78.

3.3 Variations linked to the local solar time

The variations linked to the local solar time are exhibited in Fig. 7. The amplitudes are generally in reasonable agreement for the three models, except in the case of N_2 for DTM78, which exhibits a greater amplitude. In the case of DTM94 for temperature, molecular nitrogen, atomic oxygen and helium the maximum occurs at 16, 16, 14 and 12 h local solar time, respectively, in agreement with previous determinations (Barlier et al. 1979). For MSIS86 these maxima

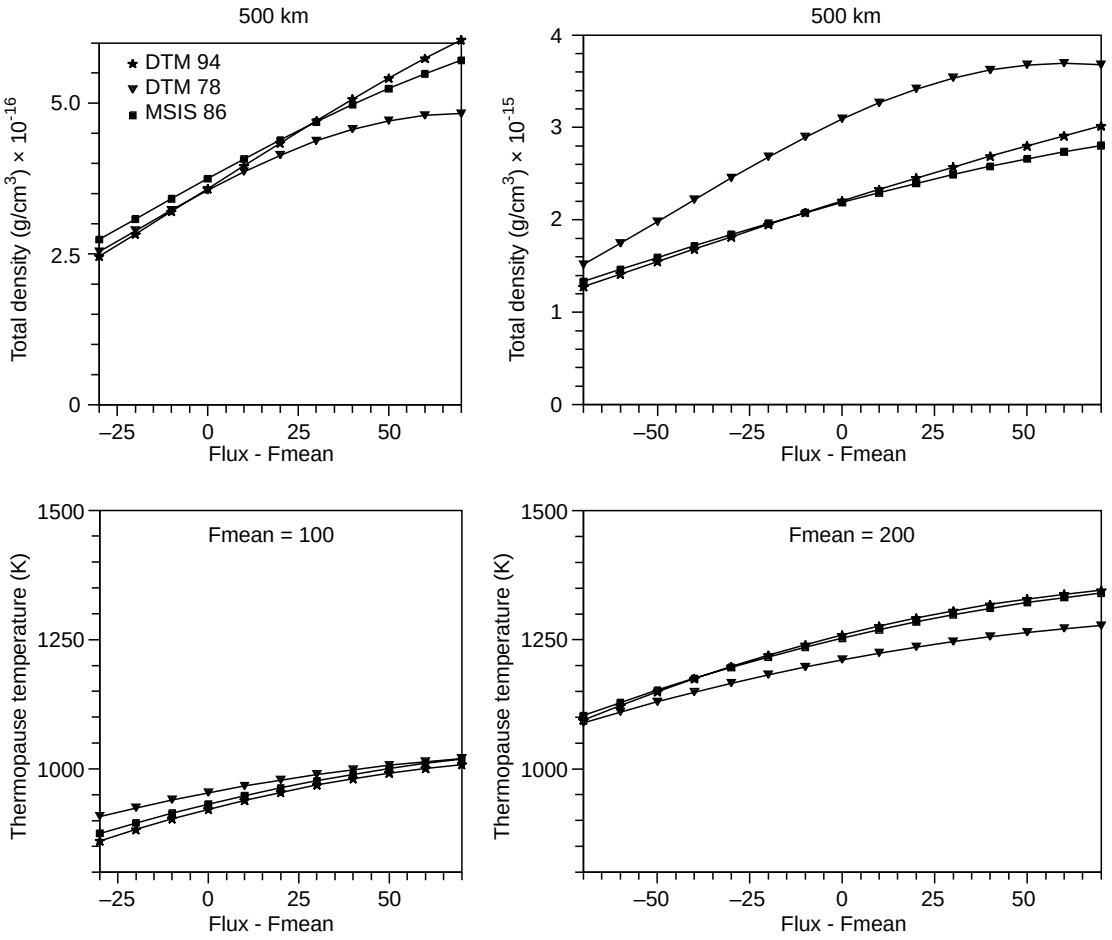

Fig. 6. Variation in thermopause temperature and in total density as a function of "$F_{10.7} - \bar{F}_{10.7}$" for two levels of solar activity

occur at 17, 13, 14 and 9 h, respectively, in reasonable agreement with DTM94. This behaviour, different for each constituent, is explained by dynamical processes. The light constituents such as helium are much more sensitive to such processes (Mayr and Harris 1977). The molecular nitrogen exhibits, for the case considered, a flat maximum between 12 and 18 h for DTM94 and a maximum at 13 h for MSIS86. It is important to emphasize that the local solar time effect strongly depends on latitude and altitude.

3.4 Variations linked to the day of the year

Variations are displayed in Fig. 8. The behaviour is very different for each component, as is already known, and a general agreement can be noted between the models considered. Temperature and N_2 are closely correlated, with a maximum during the summer time. Conversely, helium has its maximum in winter [the winter helium bulge discovered by Keating and Prior (1968)]. The semi-annual effect for atomic oxygen discovered by Paetzold and Zschörner (1961) with two maxima near the equinoxes is clearly evidenced. It is of interest to recall that this effect varies from one year to another, yielding some dispersion in fitting the data (Ill 1983). To some extent such a variation has originated in the low atmosphere, which can undergo unpredictable fluctuations. The total density follows the prevailing component at a given altitude.

3.5 Variations as a function of latitude

For spring conditions the temperature presents two maxima in the polar regions due to the precipitation of particles (Fig. 9). It is of interest to note that the MSIS86 model presents a significant and surprising asymmetry between the two hemispheres which does not appear in the two DTM models. The molecular nitrogen follows a correlated behaviour with temperature. For the atomic oxygen the behaviour is opposite with a maximum at the equator, but it has also a specific asymmetry in the MSIS86 model. The same holds for helium. On the other hand, the agreement between DTM94 and MSIS86 is good for equatorial and mid-latitudes, while DTM78 exhibits systematic differences at several latitudes.

To conclude Sect. 3, we shall see that the new version of model DTM reproduces all the main features already known of the thermospheric properties in a satisfactory way. The differences between the models can be considered as an estimate of possible accuracy.

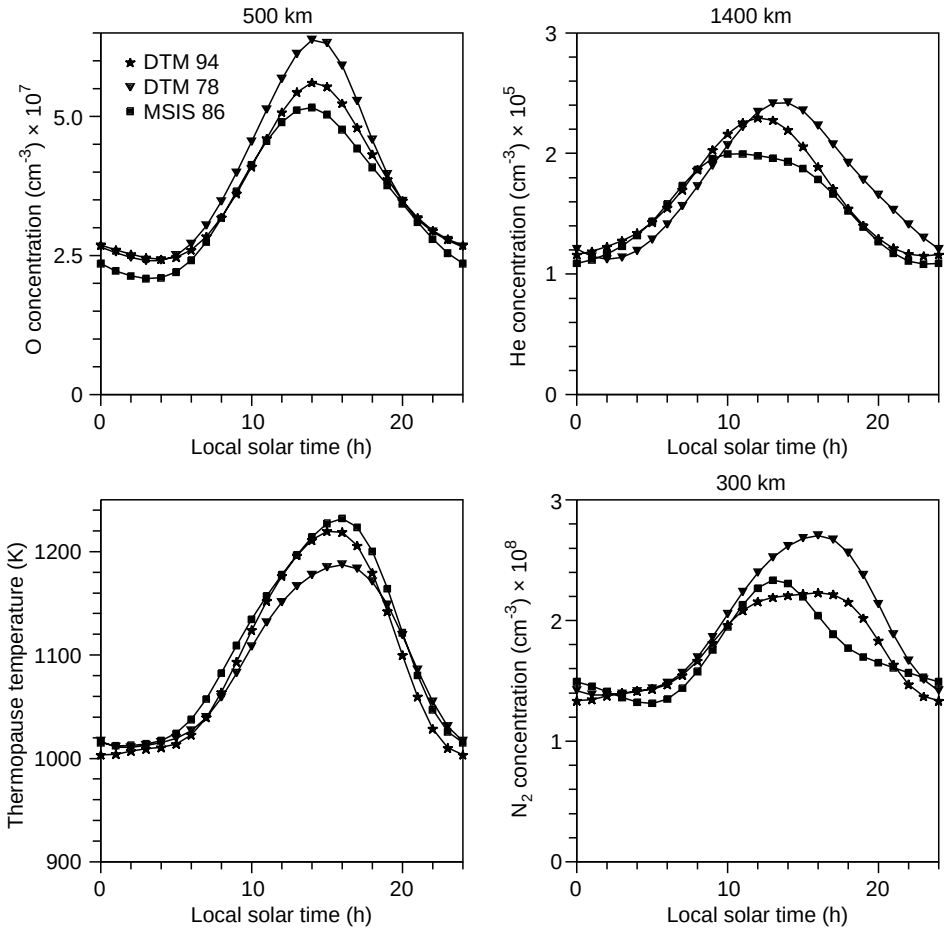

Fig. 7. Variation in thermopause temperature and in neutral composition as a function of local solar time

It is necessary to evaluate the quality of the fit by considering the distribution of residuals as a function of different parameters (observed to model value ratio, denoted f). It is also important to compare the new version of DTM with data not used in the model and to give some examples and applications of the model in fields related to space geodesy.

3.6 Comparison with data used in the models

For comparison, we have displayed the ratios (f) for temperature and total density. The results are shown in Figs. 10 and 11 for the mean solar flux, the instantaneous variations in the solar flux ($F_{10.7} - \bar{F}_{10.7}$), the geomagnetic activity and the latitude. For temperature, the fit can be considered to be satisfactory. Some problems remain for very high K_p values for the three models. For the total density the same kind of remarks can be made. Moreover, in the southern hemisphere for MSIS86, the predicted values for high latitudes are too low with respect to the data set considered here. Concerning the mean solar flux, a discrepancy has to be noted for the DTM78 model for high activity level. A drop in the f ratio can be noted for very high "$F_{10.7} - \bar{F}_{10.7}$" values.

Another way to evaluate the quality of data is to consider the mean value of the residuals (observed to model value ratios as well as their root mean squares) which are given in Table 4. The mean value between the data subsets (temperature, drag data, constituents) and the model is generally a few percent. The root mean square (rms) represents the complex but unmodelled physical effects as well as errors in modelling itself and measurement errors. Similar studies have been performed in the past by Hedin (1988) for the same kind of data.

To consider the quality of the fit more in detail, an example is given with CACTUS accelerometer data for the different parameters of the model. The mean values of the residuals and their rms are given in Table 5. Indeed, the relative precision of CACTUS as a function of measurement conditions is well known [a few percent up to 400 km (Villain 1978)] and allows some reference tests. Mean values of residuals (f ratios) are not always distributed at random. Taking into account the precision of these mean values, generally speaking better than a few percent, remaining signatures as a function of subsets of parameters can be observed up to 20% for extreme conditions. They concern mainly instantaneous daily solar flux, mean solar flux and geomagnetic activity. All these facts are of importance and show, to some extent, the limits of the modelling exercise. The data sets are not totally homogeneous to one another. Calibration problems may exist but there is also an inability of the model to represent perfectly the actual physical reality.

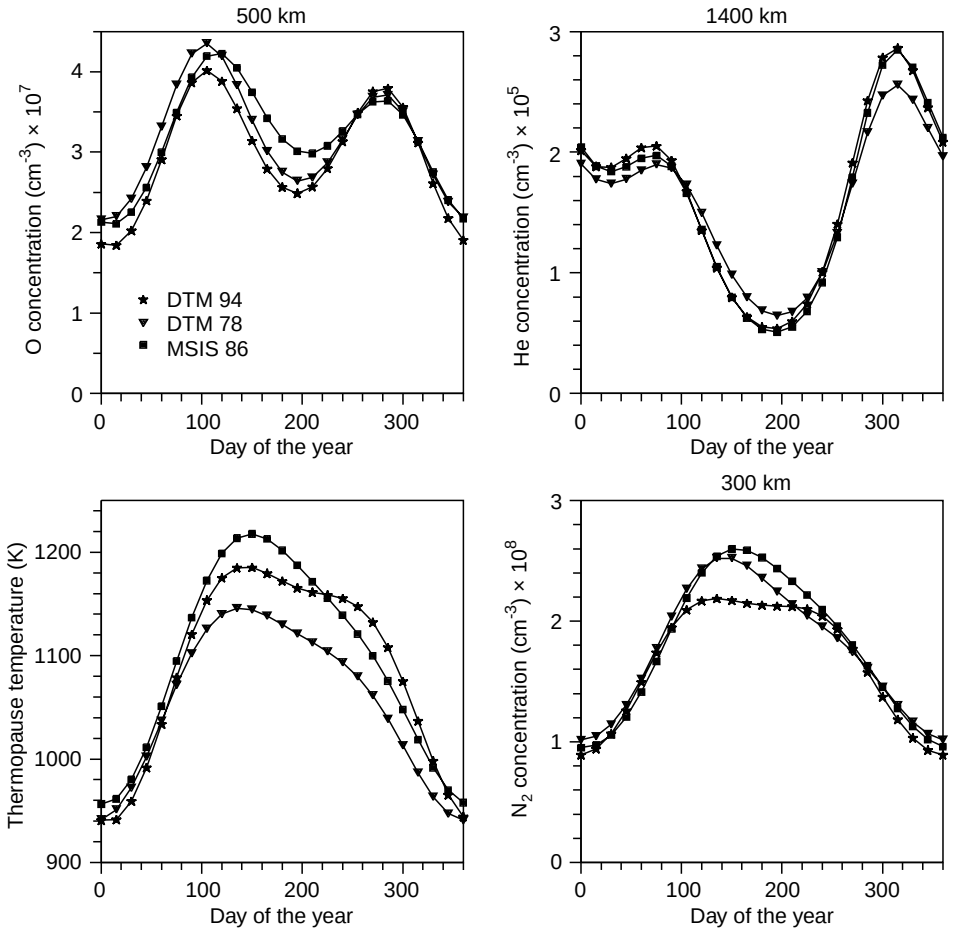

Fig. 8. Variation in thermopause temperature and in neutral composition as a function of the day of the year

Referring to Table 5, the rms ranges from 10% to 30% and is variable. When the altitude increases, the rms also increases because the density estimate depends not only on the modelling of constituents in the low thermosphere but, in addition, more and more on the modelling of temperature. Moreover, the precision of air drag measurements decreases with altitude due to the relative increase of other non-gravitational forces (Villain 1978). The rms increases also during the night as compared to the daytime, due to the decrease in the ion drag making the amplitude of air drag fluctuations more important. The precision of the CACTUS air drag measurements also decreases as a result of a less precise attitude restitution. These values increase with strong geomagnetic activity as well. K_p is in fact not a very good indicator of this activity for severe conditions, which explains the decreasing quality of the modelling (Barlier and Berger 1983). Moreover, the winds are stronger and generate perturbations. To point out the difficulty of modelling precisely the geomagnetic activity by the K_p index, an example is given from the CACTUS data during a severe geomagnetic event. The observed-to-model density ratios are displayed in Fig. 12 for individual data and for K_p greater than 6. An important dispersion appears. For a short interval of time, the factors range from 0.7 to 1.8. Should we state that the model overestimates or underestimates the physical reality? In fact, there is some inadequacy of the K_p index to represent this reality all around the Earth.

3.7 Comparison with external drag data

We have selected several data sets as a function of altitude: first at 500 km, the Intercosmos satellite IK11 (drag data kindly provided by L. Sehnal from Ondrejov Observatory), then between 600 and 1800 km [drag data from the 63 30 D balloon satellite (Slowey 1974)], and finally at very high altitude above 1700 up to 2700 km [balloon satellite data (Rousseau 1973)]. Results are given in Table 6. For the IK11 satellite the systematic high values of the mean value of the residuals are only to be interpreted as a relative calibration problem (aerodynamic coefficient has been taken equal to 2.2). The rms represents the sum of errors in modelling and in drag measurements. The main conclusion is that the three models perform the fit at a comparable level. This is also true up to 1000 km with the 63 30 D data. The rms minimum of 0.25 is obtained for the DTM94 model, which is typical of what is to be expected in predictions when including error measurements. The difference in the mean value is an indication of possible relative biases in modelling. Above 1000 km, the standard deviation increases for all the models. The greatest value is

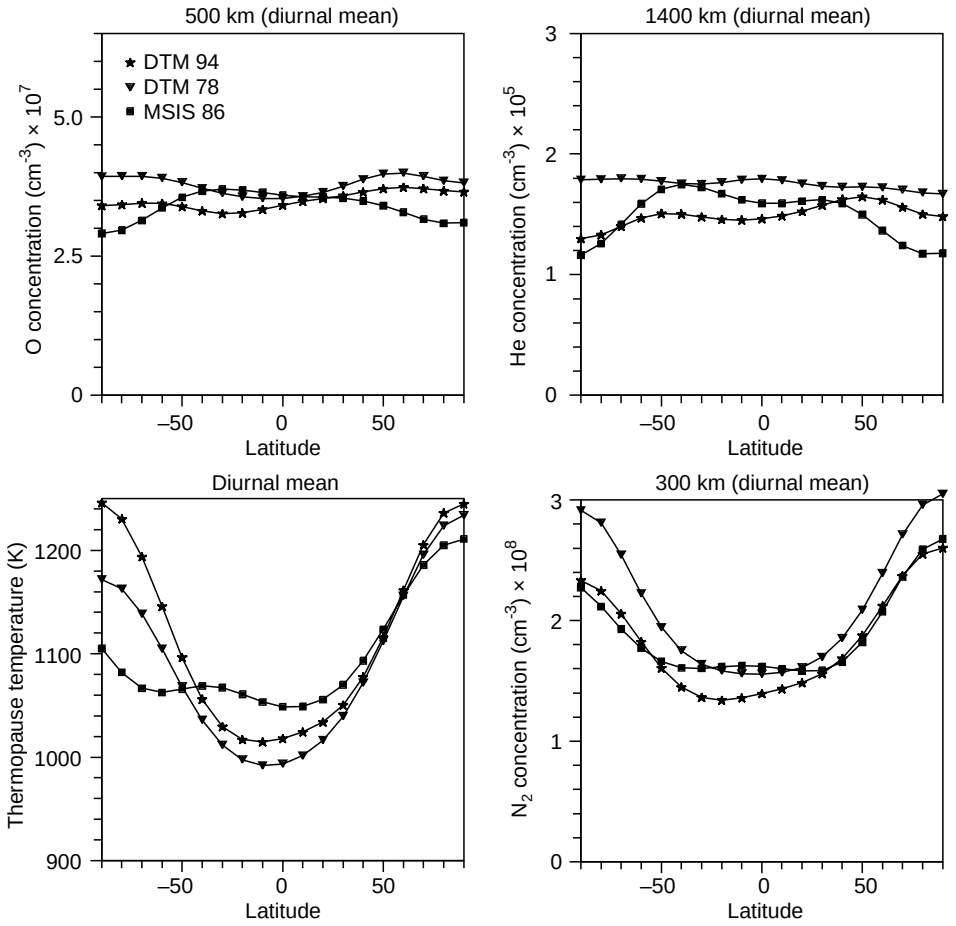

Fig. 9. Variation in thermopause temperature and in neutral composition as a function of latitude

obtained for DTM78, but here it does not include hydrogen concentrations.

The problem of satellites at very high altitudes (greater than 1700 km) is specific: high systematic values can be observed for DTM94 and MSIS86. Of course, the estimate of aerodynamic coefficients can induce systematic errors, but a recent analysis of AJISAI data (altitude 1500 km) (Sengoku et al. 1996) gives a hint of a possible origin of this fact which can be due to problems of asymmetric reflectivity or electric drag producing an along-track acceleration as observed also for LAGEOS (altitude 6000 km) (Rubincam 1987; Afonso et al. 1989). Above 1000 km, careful attention has to be paid to this kind of problem, but the amount of data is very limited and prevents drawing definitive conclusions.

Finally, all these comparisons confirm the previous conclusions on the quality of the prediction in modelling with DTM94 model.

3.8 Examples of applications in space geodesy field

Some computations of satellite trajectory determination have been performed using different thermospheric models. An example is given in Table 7 for the SPOT3 satellite (altitude 800 km) tracked with the DORIS system. Several drag scale factors (f_d) have been determined, a coefficient per 6 h, simultaneously with other classical parameters of the trajectory. The rms of satellite tracking data does not change by using one model or another, and the determined f_d coefficients are comparable. Other cases have been considered and the result is generally identical: the possibility of determining several coefficients per trajectory with systems such as GPS or DORIS makes the solution not very sensitive using a current thermospheric model rather than another one. This is even truer when reduced dynamics techniques are used, as shown by Barotto (1995). However, when old data are required in gravity field determination [e.g. laser data of the sixties and seventies (Schwintzer et al. 1997)], the tracking coverage is significantly poorer and, in such a case, the role of thermospheric models is more important.

Another interesting reason for improving thermospheric models can be found in Bruinsma et al. (1996) for determining a unique trajectory of STARLETTE satellite (perigee altitude 800 km) over 12 years. The purpose was to analyse the temporal variations of the Earth gravity field over a long time using a method developed by Exertier et al. (1994). This method aims to determine a set of "mean orbital elements" from tracking data and fit a "mean orbit" by numerical integration of "mean" differential equations of the motion in adjusting parameters such as the temporal variation of the second-degree zonal gravitational coefficient of the Earth ($\dot{J}_2$). The difficulty is to evaluate the effect of

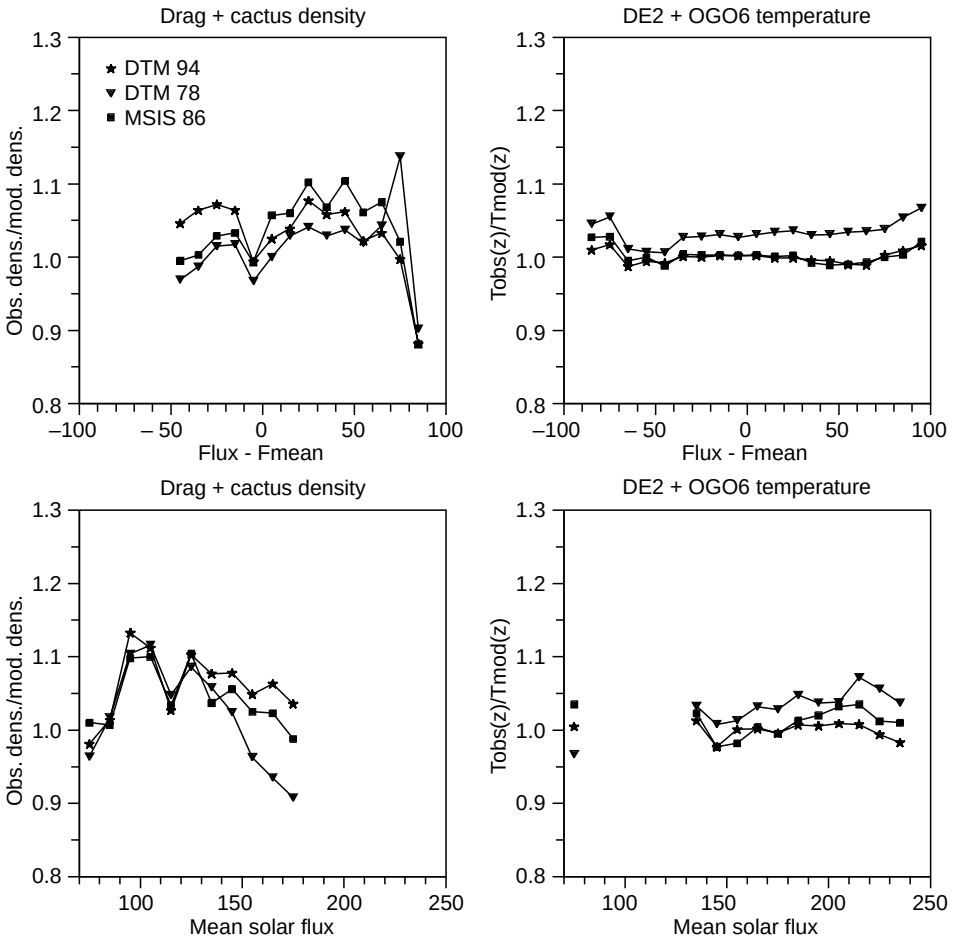

Fig. 10. For the three models studied, mean ratios between observed and model values as a function of the $\bar{F}_{10.7}$ and the "$F_{10.7} - \bar{F}_{10.7}$" indices

the atmospheric drag taking into account all the couplings between various forces. To do that, the set of "mean semi–major axes" is considered separately. Over 12 years, the observed decrease in the mean semi-major axis is about 365 m. The differences between the predicted values when extrapolating the ephemerides by using the thermospheric models DTM94, MSIS86, DTM78 and the observed values are of 19, 27 and 85 m, respectively, at the end of the 12 years. The predicted estimate by DTM94 fits the observed values to within 5%, which is very satisfactory.

On the other hand, to represent the temporal fluctuations of the semi-major axis over 12 years, at short time-scale, drag scale factors (f_d) have to be determined. DTM94 model has been used. They sometimes reach the value of 1.5 (density 50% greater than predicted), sometimes the value of 0.7 (density 30% less than predicted) (Bruinsma, private communication). The rms of these factors is of the order of 0.25. This fact emphasizes that the long-term variation represented by the slowly variable index $\bar{F}$ is much better predicted than the short variation represented by the difference index "$F - \bar{F}$".

The rms of the fit of the semi-major axis is of the order of 8 cm (Bruinsma, private communication), to be compared to the global effect of 365 m. Therefore, the long-term decrease in the semi-major axis can be estimated precisely, inducing, for example, that the indirect air drag effect on the angular parameters (the ascending node, for example) is also determined precisely. This point is crucial, making possible the precise removal of the air drag effect, because the motion of the ascending node is used for obtaining the temporal gravitational signal as $\dot{J}_2$ (Eanes and Bettadpur 1995; Exertier 1995). This shows the importance of modelling as well as possible the air drag effect and the possibility of the DTM94 model to reach such an objective. DTM94 is used presently by CNES for TOPEX/POSEIDON orbit determination (Nouël, private communication) and will be used for the new generation of the GRIM models.

4 Discussion

We have chosen a classical approach to elaborate the new version of the DTM model using the classical indices, K_p, $\bar{F}_{10.7}$, "$F_{10.7} - \bar{F}_{10.7}$". A first reason is that old space trajectory data will continue to be used, for example in gravity field modelling (Schwintzer et al. 1997) or in oceanographic altimetry data, at a time where no other indices were available. Another reason to keep the same kind of algorithm is to have a model as simple as possible for space geodesy applications with a capability to fit such or such a coefficient in order to improve a specific type of trajectory in inclination and in altitude (concept of tailored model as developed in gravity field modelling). Indeed, when combining differ-

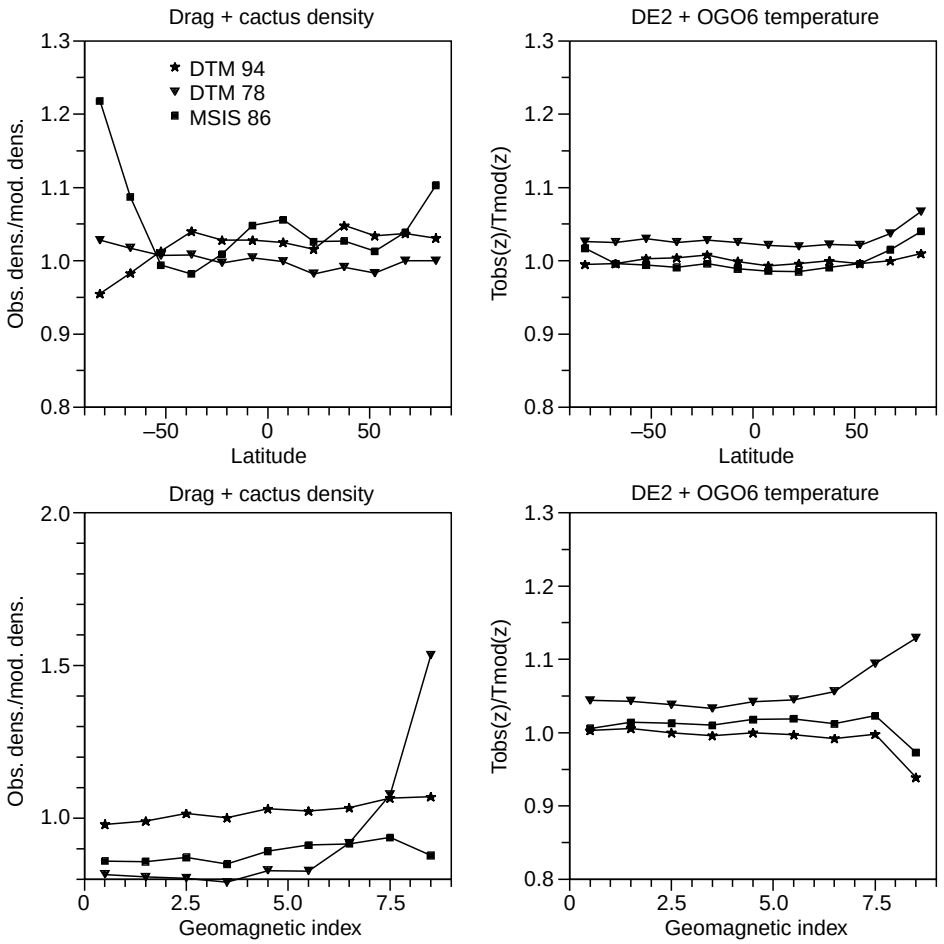

Fig. 11. For the three models studied, mean ratios between observed and model values as a function of geomagnetic activity and latitude

Table 4. For three models, mean ratios between observed and model values with their root mean squares (rms)

Data set	DTM94		DTM78		MSIS86	
	mean ratio	rms	mean ratio	rms	mean ratio	rms
Ogo-6 temperature	1.00	0.13	1.02	0.13	0.99	0.13
DE-2 temperature	1.00	0.08	1.04	0.10	1.01	0.09
Satellite drag data	1.04	0.25	1.00	0.25	1.03	0.27
CACTUS data	1.01	0.23	0.99	0.25	1.03	0.23
DE-2 N_2 density	1.01	0.30	0.81	0.35	0.87	0.35
DE-2 O density	0.99	0.22	0.85	0.34	0.99	0.26
DE-2 He density	0.99	0.22	0.79	0.31	1.00	0.22

ent subsets of thermospheric data, systematic differences between them are often visible. The least-squares procedure applied globally to all the different subsets leads to fit a solution across the data and to smooth many effects. The thermosphere is probably not stationary as a function of time as in meteorology in the very low atmosphere. In fact, we have some evidence that this is true, for example with the observation of the semi-annual effect variable from one year to another (Ill 1983). As a result, merging all the data obtained during 25 years can sometimes be unsatisfactory. For several applications it can be of interest only to represent a specific subset of data gathered over a limited interval of time. The software concept of DTM94 allows the selection of subsets of the normal equations with a set of unknowns chosen by sensitivity criteria. The flexibility of the software is an important characteristic for some uses.

From a more general point of view, the origins of the limitation of present thermospheric models have already been reviewed (Barlier and Berger 1983; Ries et al. 1993; Killeen et al. 1993; Marcos et al. 1994) but can be recalled. The energy budget which is a basic input is only represented by proxy indices. We know in fact that a variable energy is also coming from the lower atmosphere in a chaotic way not predictible by indices (planetary waves and gravity waves, for example). Energy sources coming from the ring current around the

Table 5. For different subsets of the parameters, mean ratios between observed and model densities with their root mean squares (rms). Observed densities come from CACTUS accelerometer measurements

Parameter	mean value	number of data	DTM94		DTM78		MSIS86	
			mean ratio	rms	mean ratio	rms	mean ratio	rms
K_p	0.5	9012	1.01	0.22	0.96	0.22	1.03	0.22
	2.5	17629	1.00	0.22	0.96	0.22	1.02	0.22
	4.5	5346	1.04	0.25	1.07	0.26	1.04	0.24
	6.5	405	1.10	0.28	1.35	0.40	1.16	0.33
	8.5	87	0.87	0.22	1.91	0.70	1.22	0.36
Local solar time	1.0	1963	1.08	0.30	1.04	0.30	1.05	0.29
	5.0	4613	1.05	0.28	1.03	0.29	1.00	0.26
	9.0	6225	1.01	0.21	1.05	0.27	0.99	0.22
	13.0	6423	1.00	0.17	1.03	0.18	1.06	0.20
	17.0	7492	0.97	0.21	0.94	0.22	1.03	0.20
	21.0	4380	1.01	0.25	0.88	0.23	1.02	0.24
Altitude	275.0	11256	0.98	0.13	1.06	0.17	1.00	0.13
	375.0	10165	0.98	0.20	0.98	0.23	1.00	0.19
	475.0	9204	1.02	0.27	0.94	0.28	1.04	0.26
	575.0	4741	1.14	0.32	1.03	0.34	1.16	0.35

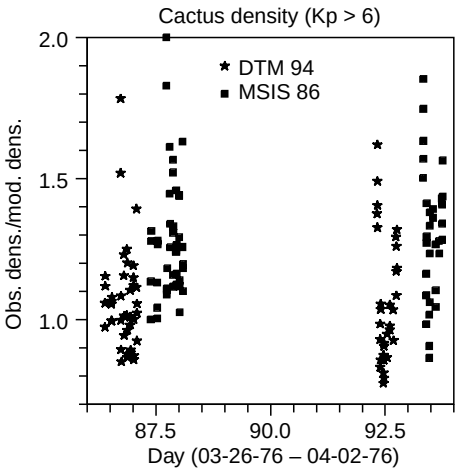

Fig. 12. During a strong geomagnetic event, ratios of individual CACTUS data to the DTM94 and MSIS86 models. For reasons of clarity, the values with respect to the MSIS86 model are conventionally shifted by 1 day

equator could be another possibility not taken into account (Almár et al. 1992). In this last paper, the energy is represented by the *Dst* index, but discussion exists now concerning its real physical meaning (Campbell 1996). Moreover, variable sinks of energy are also of importance, for example sinks inferred by NO emission

Table 7. Drag tests on SPOT 3 (10 days in April 1994)

Density model	number of measures	f_d mean	rms (f_d)	rms (mm s^{-1}) DORIS data
DTM78	34804	0.70	0.18	0.55
DTM94	34804	0.71	0.21	0.55
MSIS86	34804	0.73	0.21	0.55

(Kockarts 1980). As sinks or sources of energy are variable in an irregular and unpredictable way, they induce significant errors in modelling. Moreover, several other basic difficulties come from hypotheses never totally satisfied, for example the law of the hydrostatic equilibrium and static diffusive equilibrium as shown by observations of horizontal and vertical winds (e.g. Fauliot et al. 1993), waves at different scales, and so on. A review of these phenomena can be found, for example, in Killeen et al. (1993) and Berger and Barlier (1993). Therefore, the vertical density and temperature distribution cannot always be represented satisfactorily.

All this does not mean that any progress is not possible. In fact, progress could be envisaged with other indices such as a precipitation index (Gaposchkin and Coster 1989), an auroral index (Berger and Barlier 1981) and EUV flux, which represents an actual source of energy (Gorney 1990) that can also be monitored. Then, in the field of the classical approach (as used presently)

Table 6. For three models, mean ratios between observed and model densities with their root mean squares (rms)

Satellite	number of data	altitude (km)	mean solar flux	DTM94		DTM78		MSIS86	
				mean ratio	rms	mean ratio	rms	mean ratio	rms
IK11	378	500	130	1.28	0.37	1.17	0.35	1.24	0.37
63-30-D	145	600–1000	150	0.94	0.25	1.11	0.30	1.02	0.29
63-30-D	134	1000–1800	150	0.99	0.53	1.21	0.71	0.90	0.51
63-30-D	5	1750–2400	148	1.88	0.46			1.62	0.39
63-14-B	3	2650	145	1.22	0.63			1.67	0.73
66-54-A	8	2150–2650	150	1.69	0.67			1.57	0.64

and in spite of the limits described here, some progress may again be possible, either in the frame of tailored models as already mentioned or in the frame of Factorial Analysis (Bordet 1973) as used in the past to represent the remaining signatures. By analysing the residuals, factorial analysis may suggest empirical corrections in a simple way (Bordet 1973; Barlier et al. 1976).

On the other hand, a more physical and chemical or photochemical approach can be pursued and developed. It is not the aim of this paper to consider all these questions, but they represent a wide field of research. In any case, new thermospheric data more precise and accurate combined with external parameters (e.g. EUV solar flux) could certainly be of great importance for the future and are to be encouraged, along with new analyses.

5 Conclusion

The problem of improving thermospheric models very significantly is still open and will probably remain so for some time. However, the DTM model has certainly been improved from the first version in 1978 thanks to the introduction of new data for extreme solar conditions: for low solar activity (CACTUS data) and for high solar activity (DE2 data). Bearing in mind the use of this model in important programmes such as TOPEX/POSEIDON, SPOT and gravity field model development (GRIM models), its improvement was necessary. Moreover, the statistical vertical distribution of temperature and of the main constituents has been improved even for mid-solar activity level. From a geophysical point of view, it is a great interest of DTM models to give not only a correct estimate of the total density but also to give a correct estimate of the major constituents and of the thermopause temperature, as done in the MSIS models. From a geodetic point of view, over a long duration including solar minimum and maximum, progress has been accomplished in the trajectory determination (the STARLETTE satellite, for example) exhibiting better modelling with the slowly variable component of the solar activity ($\bar{F}$).

The present study has also discussed the errors to be expected in modelling with their dispersion as a function of geometric and solar parameters. From this aspect, the comparison performed between the MSIS86 and DTM94 models has been very instructive, allowing analysis of differences and reassessing the limits in thermospheric modelling, as well as reviewing the variability in total density, temperature and constituents (N_2, O, He).

To improve thermospheric modelling, new homogeneous measurements in thermosphere and new theoretical studies have to be encouraged. Fortunately, new missions are already scheduled: microaccelerometers will be installed on next gravity field missions (CHAMP and GRACE) to be launched around the year 2000 as well as a new atmospheric mission (TIMED) by the U.S. All this can be considered very encouraging.

Acknowledgements. This work has been supported by the "Centre National d'Etudes Spatiales", the "Ministère de la Recherche", the "Centre National de la Recherche Scientifique" in the frame of research units "Centre d'Etudes et de Recherches Géodynamiques et Astrométriques (CERGA)" and "Dynamique Terrestre et Planétaire". This support is gratefully acknowledged. The solar and geomagnetic data published by the "National Geophysical Data Center, N.O.A.A., Boulder, Colorado, USA" have been kindly provided by the "Centre de Prévision d'Activité Solaire" of Meudon Observatory. The authors want to thank F. Nouël (CNES) for his encouragement in this work as well as P. Exertier and S. Bruinsma for useful discussions. They are also indebted to the referees for valuable comments.

References

Afonso G, Barlier F, Berger C, Mignard F, Walch JJ (1985) Reassessment of the charge and neutral drag of Lageos and its geophysical implications. J Geophys Res 90: 9381–9398

Afonso G, Barlier F, Carpino M, Farinella P, Mignard F, Milani M, Nobili AM (1989) Orbital effects of Lageos seasons and eclipses. Ann Geophysicae A(7): 501–504

Almár I, Illés-Almár E, Horváth A, Kolláth Z, Bisikalo DV, Kasimenko TV (1992) Improvement of the MSIS86 and DTM thermospheric models by investigating the geomagnetic effect. Adv Space Res 12: 313–316

Banks PM, Kockarts G (1973) Working models of the thermosphere. In: (ed) Aeronomy, Part B. Academic Press, New York, pp 311–317

Barlier F, Berger C (1983) A point of view on semi-empirical thermospheric models. Planet Space Sci 31: 945–966

Barlier F, Bordet JP, Orfeuil JP (1976) Methods of analysis of satellite drag density values based upon statistical treatment and factorial analysis. Space Res 16: 161–173

Barlier F, Berger C, Falin JL, Kockarts G, Thuillier G (1978) A thermospheric model based on satellite drag data. Ann Geophysicae 34: 9–24

Barlier F, Berger C, Falin JL, Kockarts G, Thuillier G (1979) Comparison between various semi-empirical thermospheric models of the terrestrial atmosphere. J Atmos Terr Phys 41: 527–541

Barotto B (1995) Introduction de paramètres stochastiques pour améliorer l'estimation des trajectoires d'un système dynamique par une méthode de moindres carrés. Application à la détermination de l'orbite d'un satellite avec une précision centimétrique, PhD Thesis, Université Paul Sabatier de Toulouse

Bates DR (1959) Some problems concerning the terrestrial atmosphere above about the 100-km level. Proc R Soc A(253): 451–462

Berger C, Barlier F (1981) Response of the equatorial thermosphere to magnetic activity analysed with accelerometer total density data, asymmetrical structure. J Atmos Terr Phys 43: 121–133

Berger C, Barlier F (1993) Influence of thermospheric drag, winds and gravity waves on a gradiometer mission at 200 km. In: Vallance Jones A (ed) Environmental effects on spacecraft positioning and trajectories. Geophys Monogr 73, IUGG vol. 73, pp 139–150

Berger C, Ill M, Barlier F (1986) Temperature and O/N_2 ratio deduced from density scale heights at low latitudes near sunspot minimum. Temporal variations and asymmetrical features. Ann Geophysicae 4: 165–184

Berger C, Ill M, Barlier F (1988) Reassessment of the thermospheric response to geomagnetic activity at low latitudes. Ann Geophysicae 6: 541–558

Blamont JE, Luton JM (1972) Geomagnetic effect on the neutral temperature of the F region during the magnetic storm of September 1969. J Geophys Res 77: 3534–3556

Bordet JP (1973) Etude des données géophysiques – modélisations statistiques par régression factorielle, PhD thesis, Université de Paris VI
Bruinsma SL, Exertier P, Barlier F (1996) Long-arc computation for low-orbiting satellites. EGS abstract, General Assembly, Section Geodesy, The Hague
Campbell WH (1996) *Dst* is not a pure ring–current index. In: Horwitz J (ed) Space physics and aeronomy. Univ Alabama, Huntsville, AL 35899, pp in EOS, Transactions, American Geophysical Union July 23, 1996 Editor Jim Horwitz, University of Alabama pages 283–285
Carignan GR, Block BP, Maurer JC, Hedin AE, Reber CA, Spencer NW (1981) The neutral mass spectrometer on Dynamics Explorer. Space Sci Instrum 5: 429–441
Cook (1965) Satellite drag coefficient. Planet Space Sci 13: 929–946
Eanes RJ, Bettadpur SV (1995) Temporal variability of Earth's gravitational field from satellite laser ranging. In: Rapp RH, Cazenave A, Nerem RS (eds) Symp 116, Global gravity field and its temporal variations, Boulder. pp 30–42
Exertier P (1995) Variations temporelles du géoide. In: Munschy M, Sauter D, Schlich R (eds) XXIème Assemblée générale de l'union géodésique internationale, Boulder (Colorado). Edited by M. Munschy, D. Sauter and R. Schlich, pp 43–48
Exertier P, Metris G, Boudon Y, Barlier F (1994) Long-term evolution of mean orbital elements of artificial satellites. In: Schutz BE, Anderson A, Froidevaux C, Parke M (eds) Gravimetry and space techniques applied to geodynamics and ocean dynamics. Geophys Monogr 82, IUGG 17, pp 103–108
Fauliot V, Thuillier G, Herse M (1993) Observations of the F-region horizontal and vertical winds in the auroral zone. Ann Geophysicae 11: 17–28
Gaposchkin EM (1994) Calculation of satellite drag coefficients. Techn Rep 998, Mas Inst Technol Lincoln laboratory, Lexington, MA 02173
Gaposchkin EM, Coster AJ (1986) Evaluation of recent atmospheric density models. Adv Space Res 6(9): 157–165
Gaposchkin EM, Coster AJ (1989) Evaluation of thermospheric models for satellite drag and the precipitation index, Tech Rep, Mass Inst Technol Lincoln laboratory, Lexington, MA 02173
Gorney DJ (1990) Solar cycle effects on the near-earth space environment. Rev Geophys 28: 315–336
Hedin AE (1987) MSIS–86 thermospheric model. J Geophys Res 92: 4649–4662
Hedin AE (1988) High-altitude atmospheric modeling. NASA Tech Mem 100707, NASA Goddard Space Flight Center, Greenbelt, Maryland
Hedin AE, Mayr HG, Reber CA, Spencer NW, Carignan GR (1974) Empirical model of global thermospheric temperature and composition based on data from the Ogo-6 quadrupole mass spectrometer. J Geophys Res 79: 215–225
Hedin AE, Reber CA, Newton GP, Spencer NW, Brinton HC, Mayr HG, Potter WE (1977) A global thermospheric model based on mass spectrometer and incoherent scatter data MSIS2, composition. J Geophys Res 82: 2148–2156
Hedin AE, Biondi MA, Burnside RG, Hernandez G, Johnson RM, Killeen TL, Mazaudier C, Meriwether JW, Salah JE, Sica RJ, Smith RW, Spencer NW, Wickwar VB, Virdi TS (1991) Revised global model of thermosphere winds using satellite and ground-based observations. J Geophys Res 96: 7657–7688
Ill M (1983) A review of the semi-annual effect. 2nd Intercosmos seminar on upper atmospheric research, Baja, Hungary
Jacchia LG (1971) Revised static models of the thermosphere and exosphere with empirical temperature profiles. Smith Astrophys Obs Spec Rep 332: 1–113
Jacchia LG, Slowey JW (1975) A catalog of atmospheric densities from the drag on five balloon satellites. Smith Astrophys Obs Spec Rep 368: 1–416
Keating GM, Prior EJ (1968) The winter helium bulge. Space Res 8: 982–992
Killeen TL, Roble RG (1988) Thermosphere dynamics: contribution from the first 5 years of Dynamics Explorer program. Rev Geophys 26: 329–367
Killeen TL, Burns AG, Johnson RM, Marcos FA (1993) Modeling and prediction of density changes and winds affecting spacecraft trajectories. In: Vallance Jones A (ed) Environmental effects on spacecraft positioning and trajectories. Geophys Monogr 73, IUGG pp 83–109
Kockarts G (1963) L'effet de la diffusion thermique sur la distribution de l'hélium dans l'hétérosphère. Bull Acad R Belgique Classe Sci 49: 1136–1147
Kockarts G (1980) Nitric Oxyde cooling in the terrestrial thermosphere. Geophys Res Lett 7: 137–140
Kockarts G, Nicolet M (1963) L'hélium et l'hydrogène atomique au cours d'un minimum d'activité solaire. Ann Geophys 19: 370–385
Marcos FA, Bass JN, Mazzella AJ, Robinson EC (1994) Atmospheric effects on satellite orbits. In: Edited by P. K. Seidelmann and B. Kaufman. Proc Artificial Sat Theory Worksh, US Naval Obs, Washington, pp 156–186
Marshall JA, Zelensky NP, Klosko SM, Chinn DS, Luthcke SB, Rachlin KE, Williamson RG (1995) The temporal and spatial characteristics of TOPEX/POSEIDON radial orbit error. J Geophys Res 100: 25 331–25 352
Mayr HG, Harris I (1977) Diurnal variations in the thermosphere 2. Temperature, composition, and winds. J Geophys Res 82: 2628–2640
Mayr HG, Volland H (1973) Magnetic storm characteristics of the thermosphere. J Geophys Res 78: 2251–2264
Nerem RS et al. (1994) Gravity model development for TOPEX/POSEIDON: joint gravity models 1 and 2. J Geophys Res 99: 24 421–24 447
Nouël F, Berthias JP, Deleuze M, Guitart A, Laudet P, Puizzi A, Pradines D, Valorge C, Dejoie C, Susini MF, Taburiau D (1994) Precise centre national d'etudes spatiales orbits for TOPEX/POSEIDON : is reaching 2 cm still a challenge? J Geophys Res 99: 24 405–24 419
Paetzold HK, Zschörner H (1961) The structure of upper atmosphere and its variations after satellite observations. Space Res 2: 958
Prölß GW (1980) Magnetic storm associated perturbations of the upper atmosphere: recent results obtained by satellite-borne gas analysers. Rev Geophys Space Phys 18: 183–202
Ries JC, Shum CK, Tapley BD (1993) Surface forces modeling for precision orbit determination. In: Vallance Jones A (ed) Environmental effects on spacecraft positioning and trajectories. Geophys Monogr 73, IUGG 73, pp 111–124
Rousseau M (1973) Densities deduced from perturbations at high altitudes. Planet Space Sci 21: 1705–1712
Rubincam DP (1987) Lageos orbit decay due to infrared radiation from Earth. J Geophys Res, 92: 1287–1294
Scharroo R, Wakker KF, Mets GJ (1993) The orbit determination accuracy of the ERS-1 mission. In: Vol. 2 (ed) Proc 2nd ERS-1 symp – space at the service of our environment, Hamburg, Germany. ESA SP-361, pp 735–740
Schwintzer P, Reigber C, Bode A, Kang Z, Zhu SY, Massmann FH, Raimondo JC, Biancale R, Balmino G, Lemoine JM, Moynot B, Marty JC, Barlier F, Boudon Y (1997) Long-wavelength global gravity field models: GRIM4-S4, GRIM4-C4. J Geod 71: 189–208
Sehnal L (1990) Comparison of the thermosphere total density model TD 88 with CIRA 86. Adv Space Res 10(6): 27–31
Sengoku A, Cheng MK, Schutz BE, Hashimoto H (1996) Earth-heating effect on AJISAI. J Geod Soc Jpn 42: 15–27
Slowey JW (1974) Radiation-pressure and air-drag effects on the orbit of the balloon satellite 1963 30D. Smith Astrophys Obs Rep 356: 1–93
Smith AJE, Hesper ET, Kuijper DC, Mets GJ, Visser PNAM, Ambrosius BAC, Wakker KF (1996) TOPEX/POSEIDON orbit error assessment. J Geod 70: 546–553
Spencer NW, Wharton LE, Niemann HB, Hedin AE, Carignan GR, Maurer JC (1981) The Dynamics Explorer wind and temperature spectrometer. Space Sci Instrum 5: 417–428

Tapley BD, Ries JC, Davis GW, Eanes RJ, Schutz BE, Shum CK, Watkins MM, Marshall JA, Nerem RS, Putney BH, Klosko SM, Luthcke SB, Pavlis D, Williamson RG, Zelensky NP (1994) Precision orbit determination for TOPEX/POSEIDON, J Geophys Res 99: 24 383–24 404

Thuillier G, Falin JL, Barlier F (1977) Global experimental model of the exospheric temperature using optical and incoherent scatter measurements. J Atmos Terr Phys 39: 1195–1202

Villain JP (1978) Détermination de la densité du gaz thermosphérique à partir des données de l'accéléromètre Cactus. Application à l'étude des perturbations de moyenne échelle. PhD thesis, Université Pierre et Marie Curie, France

Villain JP (1980) Traitement des données brutes de l'accélé romètre Cactus. Etude des perturbations de moyenne échelle de la densité thermosphérique. Ann Geophys 36: 41–49

Volkov II (1984) Model of density for ballistic maintenance of flights of the artificial satellites of the Earth. GOST 25645.115-84, Moscow